**Energy Materials**

Article

# Metal nitride heterostructures capsulated in carbon nanospheres to accommodate lithium metal for constructing a stable composite anode

**Baichuan Ding[1], Xufei An[1], Jing Yu[1], Wei Lv[1,*], Feiyu Kang[1,2], Yan-Bing He[1,*]**

[1]Shenzhen Geim Graphene Center, Institute of Materials Research (IMR), Tsinghua Shenzhen International Graduate School, Tsinghua University, Shenzhen 518055, Guangdong, China.
[2]Laboratory of Advanced Materials, Department of Materials Science and Engineering, Tsinghua University, Beijing 100084, China.

[*]**Correspondence to:** Prof. Wei Lv, Tsinghua Shenzhen International Graduate School, Tsinghua University, University Town of Shenzhen, Nanshan District, Shenzhen 518055, Guangdong, China. E-mail: lv.wei@sz.tsinghua.edu.cn; Prof. Yan-Bing He, Tsinghua Shenzhen International Graduate School, Tsinghua University, University Town of Shenzhen, Nanshan District, Shenzhen 518055, Guangdong, China. E-mail: he.yanbing@sz.tsinghua.edu.cn

## Abstract

Although various hosts have been proposed to accommodate the Lithium (Li) metal to solve the uneven Li deposition and infinite volume change, the pulverization of the host or lithiophilic modification layer easily leads to structural damage and the poor cycling stability of the composite anode. Herein, we design a host of metal nitrides ($Mo_2N$ and WN heterostructures) nanoparticles capsulated in the hollow carbon nanospheres, which can accommodate Li metal to form a stable composite anode. The lithiophilic $Mo_2N$ guides uniform infusion and reduces the nucleation barriers of Li metal during electrochemical process. Note that the rigid WN matrix is uniformly composited with $Mo_2N$, which can suppress the pulverization of $Mo_2N$ during the repeat Li plating/stripping, ensuring the stability of regulated deposition during long cycling. High mechanical strength, uniform surface potential distribution and good electrolyte wettability of the Li metal-based composite anode guarantee the rapid Li plating/stripping kinetics. Thus, the obtained composite anode can stably cycle 1400 h at 1 mA cm$^{-2}$ and 1 mA h cm$^{-2}$ in the symmetric battery. The assembled full cells with $LiNi_{0.8}Mn_{0.1}Co_{0.1}O_2$ (NCM811) also deliver high capacity retention under the high loading (8.6 mg cm$^{-2}$) or lean electrolyte (2 μL mg$^{-1}$) condition. This work suggests a promising host structure design to construct a highly stable lithium metal anode for practical applications.

## INTRODUCTION

The energy density of conventional lithium (Li)-ion batteries (LIBs) based on the graphite anode is hard to meet the requirements of the rapid development of automobiles and portable electronic devices[1-4]. Li metal is the most promising anode for the next generation of high-energy batteries due to its ultrahigh capacity (3860 mA h g$^{-1}$) and low reduction potential (-3.04 V *vs.* the standard hydrogen electrode)[5-8]. However, the critical problems, including uncontrolled Li dendrite formation[9-12], infinite volume expansion[13,14] and severe interfacial side reactions[15-20], cause safety issues and poor stability of lithium metal batteries (LMBs). Thus far, numerous strategies have been proposed to solve the above problems, such as artificial interface construction[21-23], host structure design[24-26] and electrolyte modification engineering[27-29]. Unfortunately, most of the above works are conducted under low-capacity loadings or with flooded electrolytes, far from the harsh practical conditions[9,30].

Compared with the pure Li metal anode, the Li metal-based composite anode is more promising for applications because of its better structural stability and capability for mass production[31-33]. Various materials have been used as hosts to accommodate the Li metal, including carbon-based hosts and three-dimensional metal foams[24,33]. However, these hosts have poor interfacial compatibility with lithium[34], and thus, many lithiophilic alloys such as metal nitrides and lithium compounds are used to modify the host surface to guide the uniform plating or infusion in the hosts. Nevertheless, these lithiophilic materials usually suffer the inevitable pulverization and agglomeration during long cycling because of the reaction with Li[35,36]. Therefore, the structural integrity of lithiophilic components and host materials is important to prepare a stable Li-metal-based composite anode and realize the uniform Li plating and stripping.

Herein, we design and prepare a host of metal nitrides ($Mo_2N$ and WN heterostructures) capsulated in the hollow carbon nanospheres (denoted WN/$Mo_2$N@HCN). A composite Li metal anode was prepared by die pressing and heating the Li metal powder and WN/$Mo_2$N@HCN host together [Supplementary Figure 1]. The lithiophilic $Mo_2$N regulates the preferential metallic Li deposition inner the hollow carbon nanospheres. In addition, the rigid WN, which is well composited with $Mo_2$N, helps maintain the integrity of $Mo_2$N in cycling, ensuring continuous and stable Li deposition. The composite Li metal anode showed stable plating/stripping over 1400 h with minimal voltage divergence (16 mV at 1 mA cm$^{-2}$ and 1 mA h cm$^{-2}$). The full battery assembled with NCM811 cathode also showed excellent long cycling stability even at high mass loading (8.6 mg cm$^{-2}$) and lean electrolyte, demonstrating the practicability of such composite anode for high-performance LMBs.

## RESULTS AND DISCUSSION

The WN/$Mo_2$N@HCN host was obtained through micelle-interfacial copolymerization in the presence of soluble metal salts, followed by carbonization and nitridation[37-39]. The copolymerization of organic monomers triggers the condensation of metal salts at micelle interfaces, which achieves one-pot integration of nanoparticle preparation, encapsulation and shell formation. The WN/$Mo_2$N@HCN host shows a well-defined spherical morphology and core-shell structure [Figure 1A and B]. In addition, this process also ensures the uniform growth of WN and $Mo_2$N together to form a heterostructure-like structure due to the similar properties of the used salt precursors and simultaneous nitriding. The cavity thickness in the HCN is about ~24 nm suggested by the high-resolution TEM image [Figure 1C]. The specific surface area calculated by the Brunauer-Emmett-Teller (BET) method and the pore volume of WN/$Mo_2$N@HCN are 206 m$^2$ g$^{-1}$ and 0.35 cm$^3$ g$^{-1}$, respectively, which are much lower than those of HCN (569 m$^2$ g$^{-1}$ and 0.54 cm$^3$ g$^{-1}$). The
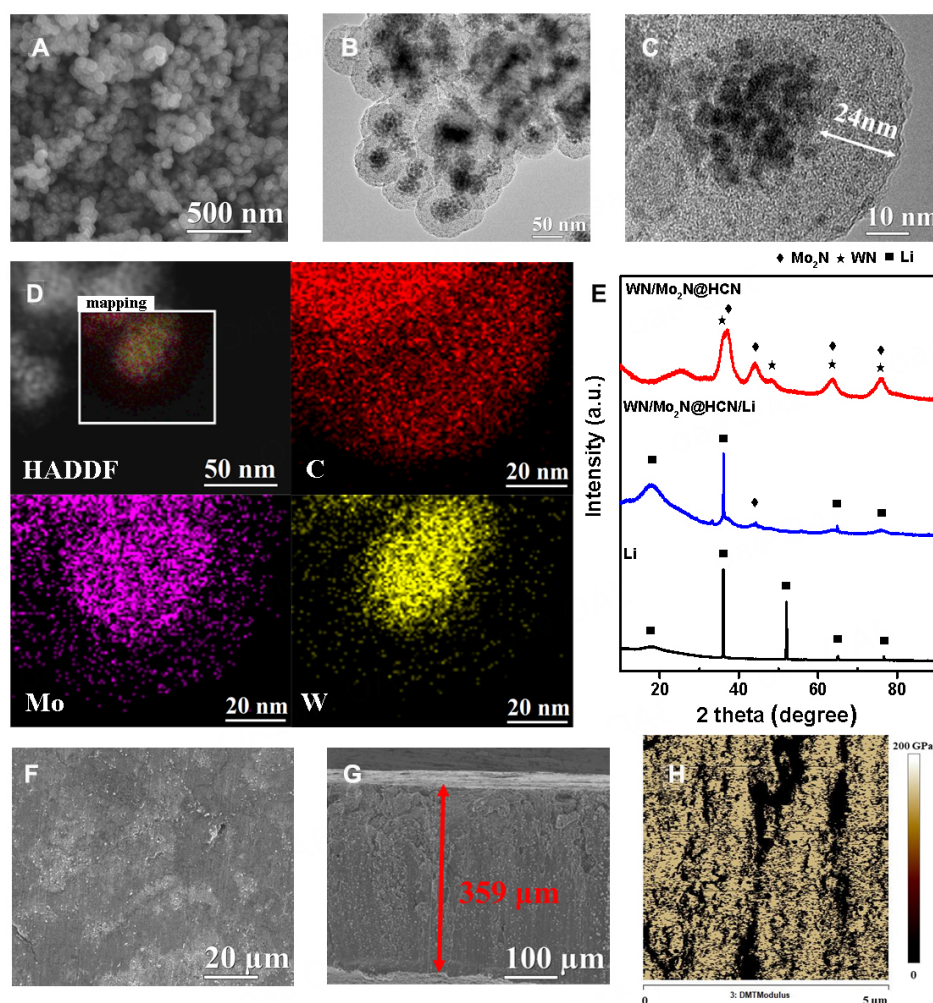
**Figure 1.** Structural characterization of WN/Mo$_2$N@HCN and the obtained Li metal composite anode. (A) SEM image, (B and C) TEM images and (D) stacked HAADF and element mappings of WN/Mo$_2$N@HCN; (E) XRD patterns, (F and G) surface and cross-sectional SEM images and (H) AFM image with Young's modulus mapping of the composite anode.

decrease in BET specific surface area and the disappearance of hysteresis loop suggest that the interior void of carbon is filled with the alloy nanoparticles after the incorporation of WN/Mo$_2$N heterostructures [Supplementary Figure 2 and Supplementary Table 1]. Furthermore, HAADF-scanning transmission electron microscopy (STEM) images and corresponding elemental mappings and diffraction peaks, as well as the X-ray diffraction pattern (XRD), suggest the formation of WN and Mo$_2$N and their uniform integration in the HCNs [Figure 1D and E], proving the formation of heterostructure-like structure between WN and Mo$_2$N. The contents of Mo and W are 12.13 wt% and 13.03 wt%, respectively, characterized by inductively coupled plasma-mass spectrometry (ICP-MS) [Supplementary Table 2]. The void space and metal nitrides guide the homogeneous Li deposition inner the HCN[40,41]. Note that the Mo$_2$N is well composited with WN, and thus, the rigid WN can help avoid pulverization and agglomeration of Mo$_2$N, ensuring stable Li deposition in HCN.

The Li metal composite anode (WN/Mo$_2$N@HCN/Li) was prepared by die pressing and heating the Li metal powder and WN/Mo$_2$N@HCN host together with different ratios (Unless specified, the mass ratio between the WN/Mo$_2$N@HCN and Li is 1:3), in which the molten Li uniformly infused into the host and formed

compact stack with high bulk density [Supplementary Table 3]. After this process, the diffraction peaks of WN/Mo$_2$N@HCN were weakened. The morphologies of the composite anode are shown in Figure 1F and G and Supplementary Figure 3A and B, which show a similar thickness (around 360 μm) to that of the prepared Li metal foil anode by Li metal powder. The surface modulus of the composite anode and lithium metal foil was characterized by an atomic force microscope (AFM). As shown in Figure 1H, the average Young's modulus of the composite anode reaches 86.0 GPa, whereas that of Li metal foil is only 10.2 GPa [Supplementary Figure 3C]. The increased mechanical strength should be ascribed to the ultrahigh hardness of metal nitrides and the carbon shell[42], which can tolerate the stress generated by the Li plating and stripping and guarantee the integrity of the composite anode[43]. The composite anode also shows a dense and smooth surface with the uniformly distributed WN/Mo$_2$N@HCN host in it, which can be confirmed by EDS elemental mapping images [Supplementary Figure 4].

The reaction between Li metal powder and WN/Mo$_2$N@HCN was investigated by X-ray photoelectron spectroscopy (XPS). The N 1s XPS peaks at 398.4 and 395.4 eV in the spectra of the composite anode [Supplementary Figure 5A] are assigned to pyridinic-N and lithium nitride formed by the partial lithiation reaction, which are not observed in that of Li metal foil [Supplementary Figure 5B][44,45]. In addition, the Li 1s XPS peak at 57.1 eV corresponds to Li-C species due to the reaction of Li and carbon [Supplementary Figure 5C and D]. The lithiophilic lithium nitride and Li-C can reduce the nucleation overpotential and induce uniform lithium deposition in cycling[46,47]. A contact angle test was conducted to explore the interfacial wettability between the liquid electrolyte and composite anode. As shown in Supplementary Figure 6, the initial contact angle was 27.7° and the droplet spread out in 10 s, but for the lithium metal foil, the contact angle was 58.6°, suggesting the improved interfacial wettability of the composite anode with the above components[48].

In order to investigate the electrochemical stability of the composite anode, the galvanostatic stripping/plating voltage profiles of symmetric cells with ether-based electrolyte were tested, as shown in Figure 2A. The composite anode exhibits stable cycling performance for more than 1400 h with an ultralow voltage hysteresis (~16 mV) without distinct voltage fluctuation at 1 mA cm$^{-2}$ and 1 mA h cm$^{-2}$. In contrast, the composite anodes of WN@HCN/Li and Mo$_2$N@HCN/Li show enlarged overpotential after 600 h and 700 h, which should be ascribed to the inferior lithiophility of WN and the pulverization of Mo$_2$N in long cycling. Note that the HCN/Li and Li metal foil anode show distinct voltage fluctuation in short cycling due to the nonuniform Li deposition, which induces uncontrollable dendrite growth. The comparison of semicircles at the high-frequency region of Nyquist plots [Figure 2B] also shows that the composite anode has the smallest electrochemical resistance due to improved ion diffusion and interfacial reaction kinetics, which is benefited from the introduction of WN/Mo$_2$N@HCN. It is shown that Mo$_2$N@HCN/Li also has a similar initial overpotential with the composite anode during the Li plating [Figure 2C], which is much smaller than those of other anodes, indicating the function of Mo$_2$N in lowering the nucleation barrier[49]. Mo$_2$N can serve as the preferred nucleation site for Li deposition, which can effectively reduce nucleation barriers, where Li can be deposited on Mo in an epitaxial manner with the lattice strain accommodated at the interface, leading to stronger Li-Mo bond than the Li-Li bond[41]. When the mass ratio of WN/Mo$_2$N@HCN and lithium powder was adjusted to 1:2 and 1:4, the cycling performance became worse than that with the ratio of 1:3 [Supplementary Figure 7]. No cracks and dead Li can be observed on the composite anode surface after 200 h stripping/plating [Figure 2D and E]. Even at a high current density of 2 mA cm$^{-2}$ and a high capacity of 2 mA h cm$^{-2}$, the cells with the composite anode still maintain excellent cycling stability for 900 cycles [Figure 2F and G].
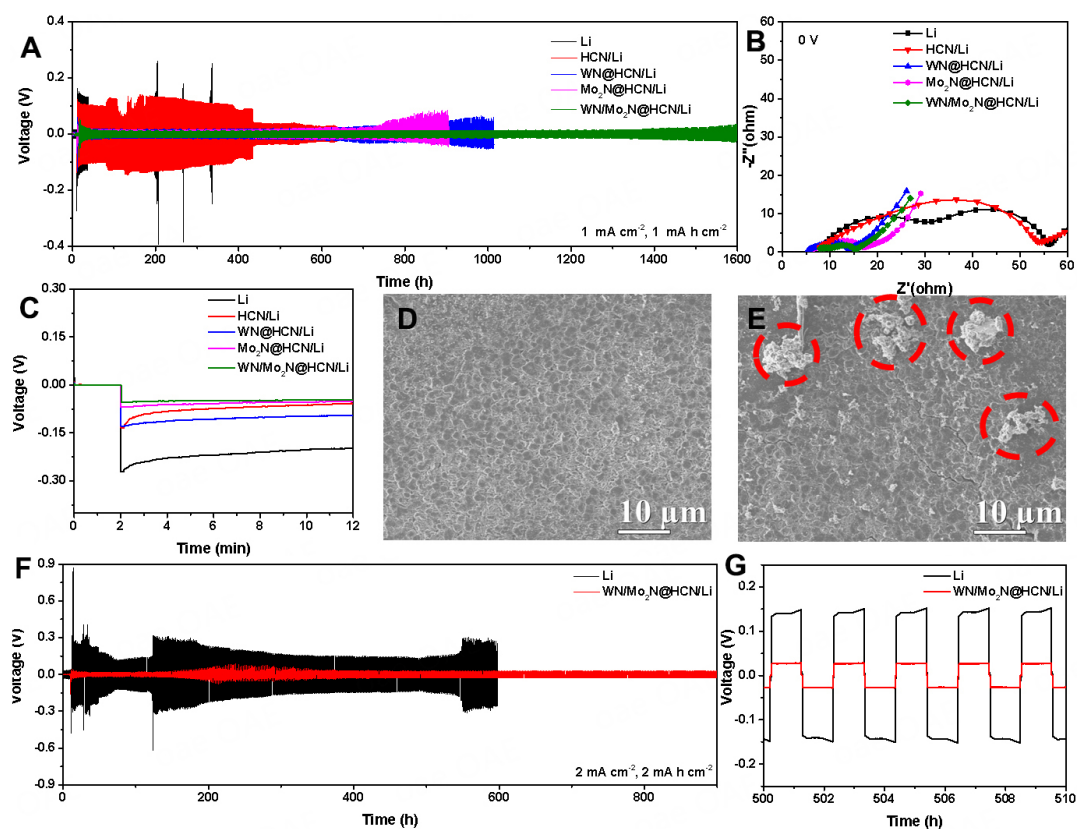
**Figure 2.** Electrochemical performance of the different anodes in symmetrical cells. (A) long-term plating/stripping profiles of composite anodes with the different hosts in symmetrical cells at 1 mA cm$^{-2}$ and 1 mA h cm$^{-2}$ and (B) the corresponding Nyquist plots; (C) overpotential profiles during the first Li plating cycle; SEM images of (D) WN/Mo$_2$N@HCN/Li and (E) pure Li metal anode after 200 h cycles; (F) long-term plating/stripping profiles of WN/Mo$_2$N@HCN/Li and pure Li metal anode in symmetrical cells at 2 mA cm$^{-2}$ and 2 mA h cm$^{-2}$ and (G) the corresponding partial enlargement at 500-510 h.

The morphology of the composite and pure Li metal anodes was characterized to reveal the different Li stripping/plating behavior at the current density of 1 mA cm$^{-2}$. With the deposition capacity of 1 mA h cm$^{-2}$, numerous disk-shaped Li pieces were evenly distributed on the composite anode surface, which finally grew into a dense and compact layer without any Li dendrite after the capacity increased to 3 mA h cm$^{-2}$ [Figure 3A and B]. In sharp contrast, unevenly distributed needle-like Li dendrites were formed on the Li metal foil anode surface under 1 mA h cm$^{-2}$ to 3 mA h cm$^{-2}$ [Figure 3C and D]. Furthermore, the AFM image in Supplementary Figure 8 shows a smooth deposition morphology with a minor surface roughness on the composite anode surface compared with that on Li metal foil anode, in agreement with the SEM images. In order to reveal the mechanism of uniform lithium deposition on different surfaces, the surface potential distributions of anodes were measured by the Kelvin probe force microscopy (KPFM), as shown in Figure 3E and F. It is seen that WN/Mo$_2$N@HCN/Li has a well-distributed surface potential with the roughness of 35.7 mV, much lower than that of the Li metal foil (70.7 mV) [Figure 3G and H], which is a benefit to uniform Li deposition, as illustrated in Figure 3I.

The smooth and flat surface of the composite anode was shown after 100 cycles in the full cell, but the surface of Li metal foil anode showed many cracks [Figure 4A and B]. The above results clearly prove that the lithiophilic metal nitride nanoparticles effectively guide homogeneous Li stripping/plating and the carbon shells well buffer volume changes to release the stress[22], which strengthens the structural stability of the composite anode during cycling. The compositions of the SEI formed on the composite and Li metal foil
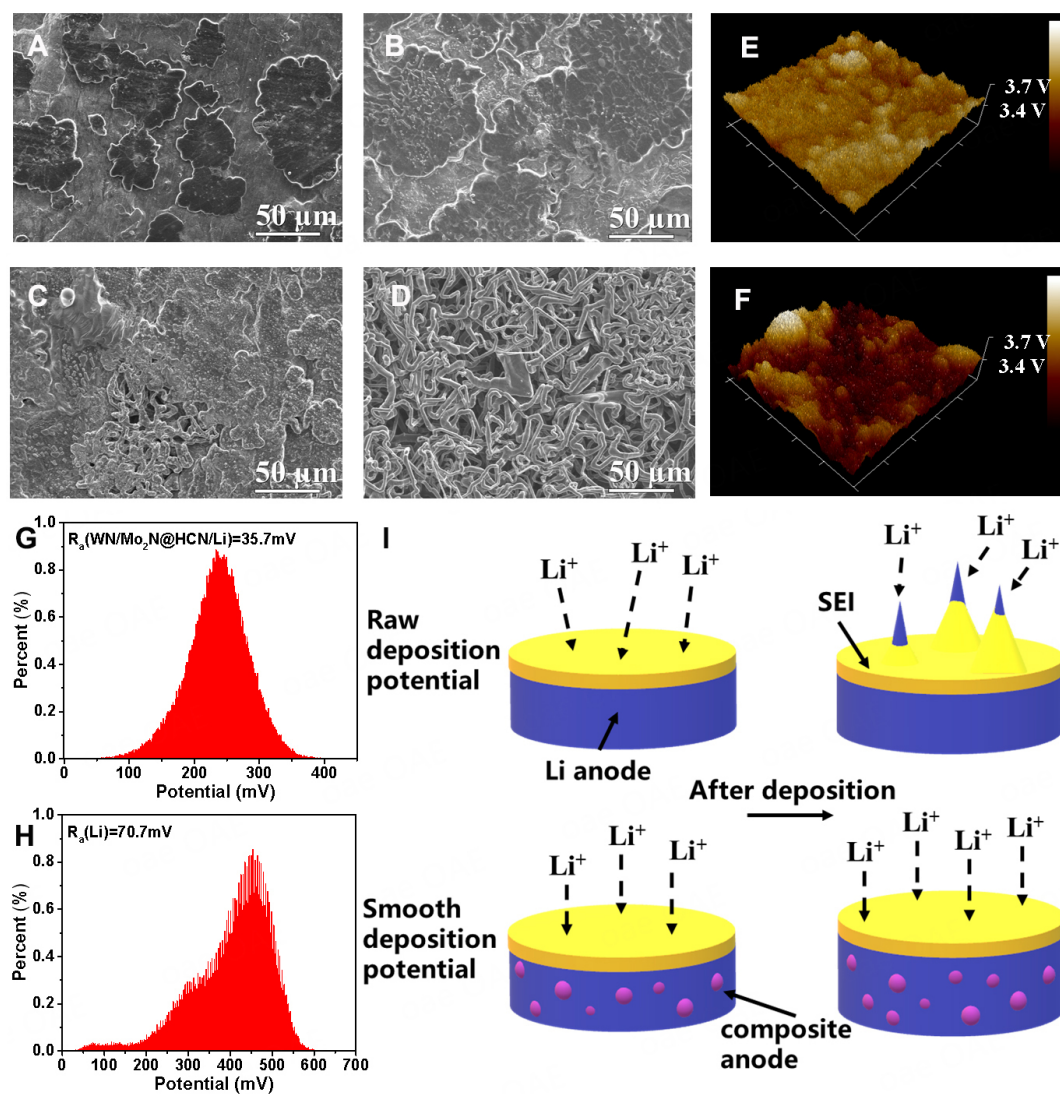
**Figure 3.** Lithium deposition behavior of different anodes. Lithium deposition morphology at 1 mA cm$^{-2}$ for (A) 1 h and (B) 3 h for the composite anode, (C) 1 h and (D) 3 h for pure Li metal anode; surface potential mappings of (E) the composite anode and (F) pure Li metal anode through Kelvin probe force microscopy (KPFM) and corresponding (G and H) statistical distribution; (I) schematic illustration of Li deposition process on these two anodes.

anodes in the carbonate electrolyte were analyzed by XPS [Figure 4C-F]. In the C 1s spectrum, the peaks at 284.4, 286.4, 288.1 and 290.2 eV correspond to the C-C/C=C, COR, $CO_3^{2-}$ and C-F species, respectively[50]. The disappearance of $Li_2CO_3$ peak in the composite anode indicates that the side reaction was suppressed significantly benefited from improved interfacial kinetics. The peaks at 687.6 and 684.7 eV in the F 1s spectrum are assigned to C-F and LiF[51]. The results show more LiF contained in the SEI formed on the composite anode surface due to the existence of lithium nitride in the composite anode, which can regulate lithium deposition behavior by boosting rapid ion transport. Such differences are also suggested by the electrochemical impedance spectroscopy [Figure 4G and H]. The interfacial impedances of Li metal foil anode not only fluctuated wildly at different cycles in the Nyquist plots, but also were larger than that of the composite anode. The apparent activation energy of Li-ions migration across SEI film on the interface was also calculated by the electrochemical impedance spectroscopy measurements under different temperatures[52]. As shown in Figure 4I, the $E_{SEI}$ of the composite anode (52.95 kJ mol$^{-1}$) is obviously lower
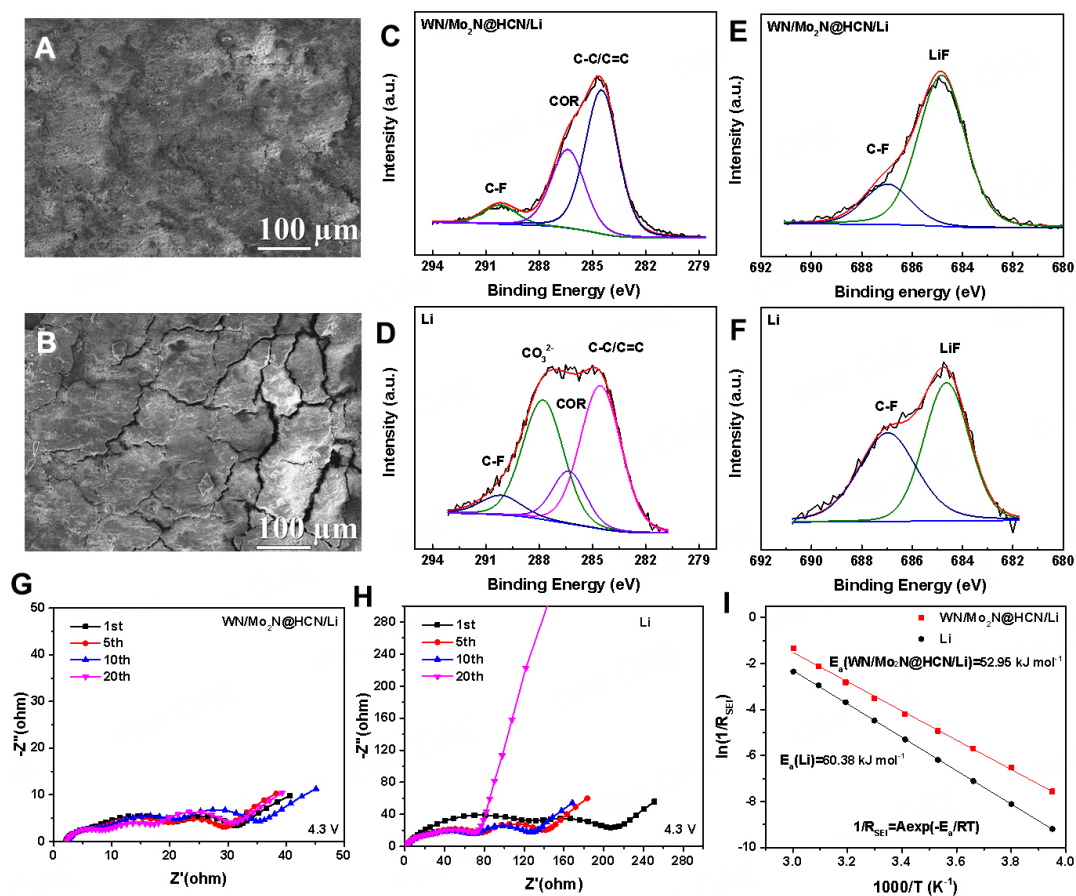
**Figure 4.** Structural stability and SEI composition of different anodes. SEM images of surface topography for (A) composite anode and (B) pure Li metal anode after cycling; high-resolution XPS analysis of (C and D) C 1s and (E and F) F 1s spectra for the composite anode and pure Li metal anode after cycling; (G and H) Nyquist plots of NCM811 full cells with the above two anodes after different cycles; (I) the $E_a$ values calculated by the electrochemical impedance spectroscopy measurements under different temperatures.

than that of Li metal foil anode (60.38 kJ mol$^{-1}$), suggesting the improved dynamics of Li-ion migration through SEI for the uniform Li deposition[53].

The full battery was assembled with NCM811 cathode to show the practicability of the composite anode. The full cell using the composite anode delivers a higher initial specific capacity of 182.4 mA h g$^{-1}$ and superior cycling performance with a capacity retention of 61.5% after 400 cycles, which are obviously higher than that of other composite anodes due to the synergistic effect of Mo$_2$N and WN heterostructures [Supplementary Figure 9], where the lithiophilic Mo$_2$N induces uniform Li deposition and the rigid WN matrix helps to suppress the pulverization and agglomeration of Mo$_2$N. Rapid decay occurred with the Mo$_2$N@HCN/Li after 300 cycles, while WN@HCN/Li and HCN/Li also delivered low capacity retention rates (51.2% and 40.9%, respectively). However, for the cell with the Li metal foil anode, the initial specific capacity and capacity retention after 400 cycles are only 162.9 mA h g$^{-1}$ and 39.5% [Figure 5A]. The coulombic efficiency of the cell with Li metal foil anode decays to 91.7% after cycling, which is much lower than that with the composite anode (99.1%), suggesting good reversibility and high lithium utilization with the WN/Mo$_2$N@HCN host.
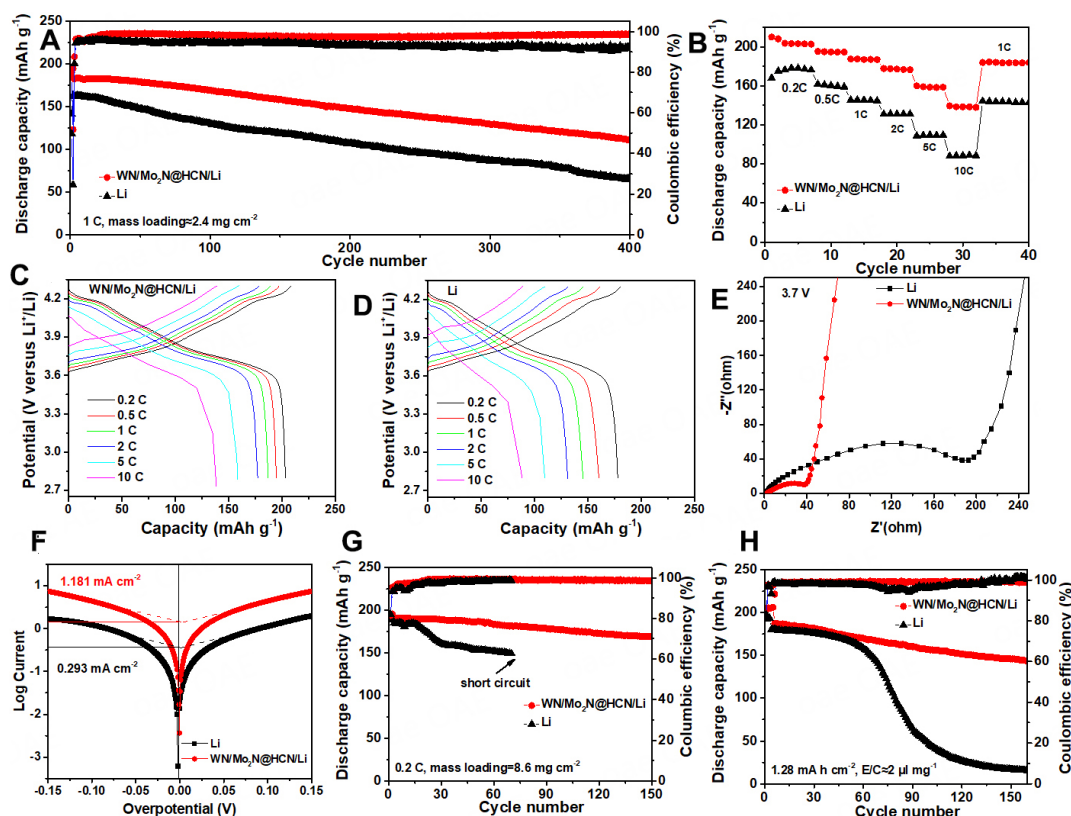
**Figure 5.** Electrochemical performance of NCM811 full cells with different anodes. (A) Cycling performance, (B) rate performance, (C and D) galvanostatic discharge-charge curves and (E) Nyquist plots of the NCM811 full cells with composite and pure Li metal anodes; (F) Tafel curves of WN/Mo$_2$N@HCN/Li and pure Li metal anodes; cycling performance of the composite anode and pure Li metal anode at (G) high cathode loading and (H) lean electrolyte amount.

The rate performances of the above two full cells were also tested from 0.2 C to 10 C, as shown in Figure 5B-D. The cell with the composite anode shows specific capacities of 203.2, 194.7, 186.9, 177.2, 158.5, and 138.5 mA h g$^{-1}$ at 0.2, 0.5,1, 2, 5, and 10 C, respectively, which are higher than the cell with Li metal foil anode. The improved rate performance is mainly ascribed to reduced electrochemical resistance indicated by the Nyquist plots [Figure 5E], where fitting results show that the composite anode has a much smaller charge transfer resistance (41.21 Ω) than that of pure Li metal anode (222.70 Ω) [Supplementary Figure 10 and Supplementary Table 4]. Furthermore, the exchange current density derived from the Tafel plots [Figure 5F] also confirms the fast interfacial reaction kinetics[54,55], where the cell with the composite anode shows about four times higher exchange current density than that with Li metal foil anode (1.181 mA cm$^{-2}$ *vs.* 0.293 mA cm$^{-2}$). Besides, the cell with the composite anode also demonstrates stable cycling performance under high-loading cathode (8.6 mg cm$^{-2}$) and lean electrolyte (E/C ratio of 2 μL mg$^{-1}$), revealing high capacity retention of 88.2% and 77.1% after 150 cycles, respectively [Figure 5G and H]. In contrast, rapid capacity decay followed by the failure of cells occurred under the same test conditions for the cells with Li metal foil anode, which should be attributed to active lithium loss and electrolyte consumption resulting from uncontrollable lithium dendrites and severe interfacial side reactions.

## CONCLUSIONS

In summary, a host of metal nitrides (Mo$_2$N and WN heterostructure) capsulated in the hollow carbon nanospheres was developed, which can accommodate Li metal to form a composite anode with excellent stability. The lithiophilic Mo$_2$N guides the uniform infusion and the electrochemical plating of Li in HCN.

At the same time, WN, which is well composited with $Mo_2N$, acts as a rigid matrix to conquer the pulverization of $Mo_2N$ during the Li plating/stripping, enhancing the structural stability of the host and regulated deposition during long cycling. The obtained composite anode thus shows excellent electrochemical performance and stability. The symmetric battery can work stably for more than 1400 h at 1 mA $cm^{-2}$ with a capacity of 1 mA h $cm^{-2}$. Furthermore, the assembled full battery with NCM811 cathode maintains a capacity of 112.2 mA h $g^{-1}$ after 400 cycles with a high coulombic efficiency of 99.1%. Even with a high-loading cathode and lean electrolyte conditions, the full batteries still show good cycling stability. This work provides a simple way to prepare a stable Li metal-based composite anode for lithium metal batteries.

## DECLARATIONS

### Authors' contributions
Contributed equally to this work: Ding B, An X
Conceived the concept and directed the research: He YB, Lv W
Carried out the synthesis and characterization: Ding B, An X, Yu J
Gave advice to the research: Lv W, Kang F
Wrote the manuscript: Ding B, He YB

### Availability of data and materials
Supplementary Information associated with this article can be found in the online version.

### Financial support and sponsorship

### Conflicts of interest
All authors declared that there are no conflicts of interest.

### Ethical approval and consent to participate
Not applicable.

### Consent for publication
Not applicable.

### Copyright

## REFERENCES
1. Grey CP, Tarascon JM. Sustainability and in situ monitoring in battery development. *Nat Mater* 2016;16:45-56.  DOI  PubMed
2. Larcher D, Tarascon JM. Towards greener and more sustainable batteries for electrical energy storage. *Nat Chem* 2015;7:19-29.  DOI  PubMed
3. Scrosati B, Hassoun J, Sun Y. Lithium-ion batteries. A look into the future. *Energy Environ Sci* 2011;4:3287.  DOI
4. Tarascon JM, Armand M. Issues and challenges facing rechargeable lithium batteries. *Nature* 2001;414:359-67.  DOI  PubMed
5. Albertus P, Babinec S, Litzelman S, Newman A. Status and challenges in enabling the lithium metal electrode for high-energy and low-cost rechargeable batteries. *Nat Energy* 2018;3:16-21.  DOI
6. Cheng XB, Zhang R, Zhao CZ, Zhang Q. Toward safe lithium metal anode in rechargeable batteries: a review. *Chem Rev* 2017;117:10403-73.  DOI  PubMed
7. Lin D, Liu Y, Cui Y. Reviving the lithium metal anode for high-energy batteries. *Nat Nanotechnol* 2017;12:194-206.  DOI  PubMed

8.    Liu DH, Bai Z, Li M, et al. Developing high safety Li-metal anodes for future high-energy Li-metal batteries: strategies and perspectives. *Chem Soc Rev* 2020;49:5407-45.  DOI  PubMed

9.    Chen XR, Zhao BC, Yan C, Zhang Q. Review on Li deposition in working batteries: from nucleation to early growth. *Adv Mater* 2021;33:e2004128.  DOI  PubMed

10.   Lu Y, Tu Z, Archer LA. Stable lithium electrodeposition in liquid and nanoporous solid electrolytes. *Nat Mater* 2014;13:961-9.  DOI  PubMed

11.   Zhang L, Yang T, Du C, et al. Lithium whisker growth and stress generation in an in situ atomic force microscope-environmental transmission electron microscope set-up. *Nat Nanotechnol* 2020;15:94-8.  DOI  PubMed

12.   Zou P, Sui Y, Zhan H, et al. Polymorph evolution mechanisms and regulation strategies of lithium metal anode under multiphysical fields. *Chem Rev* 2021;121:5986-6056.  DOI  PubMed

13.   Li M, Lu J, Chen Z, Amine K. 30 years of lithium-ion batteries. *Adv Mater* 2018;30:e1800561.  DOI  PubMed

14.   Lu J, Chen Z, Pan F, Cui Y, Amine K. High-performance anode materials for rechargeable lithium-ion batteries. *Electrochem Energ Rev* 2018;1:35-53.  DOI

15.   Cao X, Ren X, Zou L, et al. Monolithic solid-electrolyte interphases formed in fluorinated orthoformate-based electrolytes minimize Li depletion and pulverization. *Nat Energy* 2019;4:796-805.  DOI

16.   Li Y, Li Y, Pei A, et al. Atomic structure of sensitive battery materials and interfaces revealed by cryo-electron microscopy. *Science* 2017;358:506-10.  DOI  PubMed

17.   Liu T, Lin L, Bi X, et al. In situ quantification of interphasial chemistry in Li-ion battery. *Nat Nanotechnol* 2019;14:50-6.  DOI  PubMed

18.   Wu H, Jia H, Wang C, Zhang J, Xu W. Recent progress in understanding solid electrolyte interphase on lithium metal anodes. *Adv Energy Mater* 2021;11:2003092.  DOI

19.   Yan C, Xu R, Xiao Y, et al. Toward critical electrode/electrolyte interfaces in rechargeable batteries. *Adv Funct Mater* 2020;30:1909887.  DOI

20.   Zhou Y, Su M, Yu X, et al. Real-time mass spectrometric characterization of the solid-electrolyte interphase of a lithium-ion battery. *Nat Nanotechnol* 2020;15:224-30.  DOI  PubMed

21.   Yu Z, Cui Y, Bao Z. Design principles of artificial solid electrolyte interphases for lithium-metal anodes. *Cell Rep Phys Sci* 2020;1:100119.  DOI

22.   Zheng G, Lee SW, Liang Z, et al. Interconnected hollow carbon nanospheres for stable lithium metal anodes. *Nat Nanotechnol* 2014;9:618-23.  DOI  PubMed

23.   Gao Y, Yan Z, Gray JL, et al. Polymer-inorganic solid-electrolyte interphase for stable lithium metal batteries under lean electrolyte conditions. *Nat Mater* 2019;18:384-9.  DOI  PubMed

24.   Yang CP, Yin YX, Zhang SF, Li NW, Guo YG. Accommodating lithium into 3D current collectors with a submicron skeleton towards long-life lithium metal anodes. *Nat Commun* 2015;6:8058.  DOI  PubMed  PMC

25.   Chen H, Yang Y, Boyle DT, et al. Free-standing ultrathin lithium metal-graphene oxide host foils with controllable thickness for lithium batteries. *Nat Energy* 2021;6:790-8.  DOI

26.   Wan M, Kang S, Wang L, et al. Mechanical rolling formation of interpenetrated lithium metal/lithium tin alloy foil for ultrahigh-rate battery anode. *Nat Commun* 2020;11:829.  DOI  PubMed  PMC

27.   Jie Y, Ren X, Cao R, Cai W, Jiao S. Advanced liquid electrolytes for rechargeable Li metal batteries. *Adv Funct Mater* 2020;30:1910777.  DOI

28.   Jin C, Liu T, Sheng O, et al. Rejuvenating dead lithium supply in lithium metal anodes by iodine redox. *Nat Energy* 2021;6:378-87.  DOI

29.   Yang K, Chen L, Ma J, et al. Stable interface chemistry and multiple ion transport of composite electrolyte contribute to ultra-long cycling solid-state $LiNi_{0.8}Co_{0.1}Mn_{0.1}O_2$/lithium metal batteries. *Angew Chem Int Ed* 2021;60:24668-75.  DOI  PubMed

30.   Li G. Regulating mass transport behavior for high-performance lithium metal batteries and fast-charging lithium-ion batteries. *Adv Energy Mater* 2021;11:2002891.  DOI

31.   Zhou F, Li Z, Lu YY, et al. Diatomite derived hierarchical hybrid anode for high performance all-solid-state lithium metal batteries. *Nat Commun* 2019;10:2482.  DOI  PubMed  PMC

32.   Krauskopf T, Mogwitz B, Rosenbach C, Zeier WG, Janek J. Diffusion limitation of lithium metal and Li-Mg alloy anodes on LLZO type solid electrolytes as a function of temperature and pressure. *Adv Energy Mater* 2019;9:1902568.  DOI

33.   Zhang R, Chen X, Shen X, et al. Coralloid carbon fiber-based composite lithium anode for robust lithium metal batteries. *Joule* 2018;2:764-77.  DOI

34.   Duan J, Zheng Y, Luo W, et al. Is graphite lithiophobic or lithiophilic? *Natl Sci Rev* 2020;7:1208-17.  DOI  PubMed  PMC

35.   Lu D, Shao Y, Lozano T, et al. Failure mechanism for fast-charged lithium metal batteries with liquid electrolytes. *Adv Energy Mater* 2015;5:1400993.  DOI

36.   Zhan Y, Shi P, Ma X, et al. Failure mechanism of lithiophilic sites in composite lithium metal anode under practical conditions. *Adv Energy Mater* 2022;12:2103291.  DOI

37.   Xu F, Ding B, Qiu Y, et al. Generalized domino-driven synthesis of hollow hybrid carbon spheres with ultrafine metal nitrides/oxides. *Matter* 2020;3:246-60.  DOI

38.   Xu F, Qu C, Lu Q, et al. Atomic Sn-enabled high-utilization, large-capacity, and long-life Na anode. *Sci Adv* 2022;8:eabm7489.  DOI

PubMed  PMC

39.  Xu F, Tang Z, Huang S, et al. Facile synthesis of ultrahigh-surface-area hollow carbon nanospheres for enhanced adsorption and energy storage. *Nat Commun* 2015;6:7221.  DOI

40.  Zhao Q, Hao X, Su S, et al. Expanded-graphite embedded in lithium metal as dendrite-free anode of lithium metal batteries. *J Mater Chem A* 2019;7:15871-9.  DOI

41.  Luo L, Li J, Yaghoobnejad Asl H, Manthiram A. A 3D lithiophilic$Mo_2$N-modified carbon nanofiber architecture for dendrite-free lithium-metal anodes in a full cell. *Adv Mater* 2019;31:e1904537.  DOI  PubMed

42.  Wang S, Yu X, Lin Z, et al. Synthesis, crystal structure, and elastic properties of novel tungsten nitrides. *Chem Mater* 2012;24:3023-8.  DOI

43.  Zhang W, Fan L, Tong Z, et al. Stable Li-metal deposition via a 3D nanodiamond matrix with ultrahigh young's modulus. *Small Methods* 2019;3:1900325.  DOI

44.  Yu J, Shi K, Zhang S, et al. A lithium nucleation-diffusion-growth mechanism to govern the horizontal deposition of lithium metal anode. *Sci China Mater* 2021;64:2409-20.  DOI

45.  Xu F, Ding B, Qiu Y, et al. Hollow carbon nanospheres with developed porous structure and retained n doping for facilitated electrochemical energy storage. *Langmuir* 2019;35:12889-97.  DOI  PubMed

46.  Shi P, Li T, Zhang R, et al. Lithiophilic $LiC_6$ layers on carbon hosts enabling stable Li metal anode in working batteries. *Adv Mater* 2019;31:e1807131.  DOI  PubMed

47.  Zhu J, Cai D, Li J, et al. In-situ generated $Li_3$N/Li-Al alloy in reduced graphene oxide framework optimizing ultra-thin lithium metal electrode for solid-state batteries. *Energy Stor Mater* 2022;49:546-54.  DOI

48.  Ye W, Pei F, Lan X, et al. Stable nano-encapsulation of lithium through seed-free selective deposition for high-performance Li battery anodes. *Adv Energy Mater* 2020;10:1902956.  DOI

49.  Yan K, Lu Z, Lee H, et al. Selective deposition and stable encapsulation of lithium through heterogeneous seeded growth. *Nat Energy* 2016;1:16010.  DOI

50.  Rustomji CS, Yang Y, Kim TK, et al. Liquefied gas electrolytes for electrochemical energy storage devices. *Science* 2017;356:eaal4263.  DOI  PubMed

51.  Huang Z, Ren J, Zhang W, et al. Protecting the Li-metal anode in a Li-$O_2$ battery by using boric acid as an sei-forming additive. *Adv Mater* 2018;30:e1803270.  DOI

52.  Zhang W, Wu Q, Huang J, et al. Colossal granular lithium deposits enabled by the grain-coarsening effect for high-efficiency lithium metal full batteries. *Adv Mater* 2020;32:e2001740.  DOI  PubMed

53.  Li S, Wang XS, Han B, et al. Ultrathin and high-modulus $LiBO_2$ layer highly elevates the interfacial dynamics and stability of lithium anode under wide temperature range. *Small* 2022;18:e2106427.  DOI  PubMed

54.  Wang Y, Liu F, Fan G, et al. Electroless formation of a fluorinated Li/Na hybrid interphase for robust lithium anodes. *J Am Chem Soc* 2021;143:2829-37.  DOI

55.  Fu L, Wang X, Wang L, et al. A salt-in-metal anode: stabilizing the solid electrolyte interphase to enable prolonged battery cycling. *Adv Funct Mater* 2021;31:2010602.  DOI